The Astrophysical Journal, 722:1514–1521, 2010 October 20 doi:10.1088/0004-637X/722/2/1514

THE OPTICAL DEPTH OF WHITE-LIGHT FLARE CONTINUUM

Hugh Potts, Hugh Hudson[1], Lyndsay Fletcher, and Declan Diver
Department of Physics and Astronomy, University of Glasgow, G12 8QQ, UK; hugh@astro.gla.ac.uk
Received 2010 April 4; accepted 2010 August 21; published 2010 September 30

ABSTRACT

The white-light continuum emission of a solar flare remains a puzzle as regards its height of formation and its emission mechanism(s). This continuum and its extension into the near-UV contain the bulk of the energy radiated by a flare, and so its explanation is a high priority. We describe a method to determine the optical depth of the emitting layer and apply it to the well-studied flare of 2002 July 15, making use of MDI pseudo-continuum intensity images. We find the optical depth of the visible continuum in all flare images, including an impulsive ribbon to be small, consistent with the observation of Balmer and Paschen edges in other events.

Key words: Sun: flares – Sun: photosphere

Online-only material: color figures

1. INTRODUCTION

The first-observed feature of a solar flare, the "white-light" continuum, remains enigmatic to the present day. Nevertheless, it (and the related near-UV continuum) contains the bulk of a flare's radiant energy, so that an understanding of how it forms would help a great deal in our understanding of flare physics. Indeed, understanding the most important component of the energy of a flare must in fact be the single most important problem in flare physics (e.g., Neidig 1989).

The difficulties limiting our observational knowledge are several. First, the continuum excess over the bright photospheric emission only rises to some tens of percent even in the most powerful flares, and there are both practical (the image contrasts of sunspots) and intrinsic (convection and other solar "noise," such as the *p*-modes) limits to the photometric precision. Also, the strong variability both in space and time of the white-light emission has made it difficult to obtain a good characterization of the spectrum of the emission. The data that do exist suggest two types of white-light flare continuum: class (a), associated with the impulsive phase and which appears to show particle signatures, and class (b), which is featureless (Boyer et al. 1985).[2]

We do know that the white-light continuum can have a strong association with the hard X-ray emission in the impulsive phase of the flare, both temporal (Rust & Hegwer 1975; Hudson et al. 1992; Neidig & Kane 1993) and spatial (e.g., Metcalf et al. 2003; Xu et al. 2006). This indeed was one of the first motivations for the "thick-target model," which associates the chromospheric and photospheric effects of a flare with the energy losses of high-energy particles (Najita & Orrall 1970; Švestka 1970) and specifically the electrons in the 10–100 keV range (Hudson 1972). The energetics of the electrons matches well (Hudson 1972; Fletcher et al. 2007), at least, to the extent that we understand the energy in the white-light and UV continuum. Recent observations of the bolometric luminosity of a solar flare (Woods et al. 2004; Kretzschmar et al. 2010; Quesnel et al. 2010) have proven to be consistent with the idea that the white-light continuum and its UV extension dominate the flare luminosity, and furthermore that this luminosity appears in the impulsive phase. Thus, mechanisms that can explain white-light continuum formation must have a link to the non-thermal electrons responsible for hard X-ray emission in the impulsive phase.

The theoretical quandary that has blocked a full understanding is that the 10–100 keV electrons of the impulsive phase cannot penetrate as deeply as the non-flaring visible photosphere (the level for which the optical depth at 5000 Å $\tau_{5000} = 1$, where one might naively expect the white-light flare continuum to originate). This problem was exacerbated in the extreme when Xu et al. (2004) found significant contrast for flare emission even at 1.56 μ, nominally the "opacity minimum" region of the spectrum, which according to standard modeling would form actually *below* $\tau_{5000} = 1$. Several possible solutions to this quandary have been proposed, viz,

1. overionization in the chromosphere, at the stopping depth of electrons of sufficient total energy, may enhance the continuum adequately across the spectrum (Hudson 1972; Aboudarham & Henoux 1986);
2. the radiative backwarming due to hydrogen recombination at the primary stopping height of the thick-target electrons may heat the photosphere itself sufficiently to produce the observed continuum (Machado et al. 1989);
3. the continuum may result from proton energy losses rather than electrons; protons at a few MeV energy penetrate more deeply (Najita & Orrall 1970);
4. the thick-target model may be wrong, and both the hard X-ray emission and the visible continuum come from a deeper layer excited by some other mechanism (e.g., Unsöld 1968).

Of these possibilities, items (1) and (2) make clear predictions for the optical depth of the visible continuum; an overionized layer in the chromosphere will produce an optically thin spectrum of recombination radiation, while backwarming by definition would have a blackbody spectral distribution. What spectroscopy does exist favors (1) to a certain extent, because the best impulsive-phase optical spectroscopy suggests the presence of the Balmer jump and even the Paschen jump (Neidig & Wiborg 1984). The other categories of explanation, (3) and (4), are more problematic since so little theoretical work has been done, but it is clear that the classical thick-target model needs revision because the modern data require beam intensities

[1] Also at SSL, UC Berkeley, CA 94720, USA.
[2] These classes are also called type I and type II (Machado et al. 1986).

greater than those which seem physically plausible (Fletcher & Hudson 2008; Brown et al. 2009).

The backwarming mechanism deserves special mention because as Machado et al. (1989) point out, it *must* happen: Balmer radiation from the chromosphere emitted downward can freely penetrate to the upper photosphere (the temperature-minimum region), heating the medium up to radiative equilibrium. Then, the usual H^- opacity at a slightly elevated temperature (say, 300 K) could produce the white-light flare. This process would be independent of the optical depth of the primary emitter in the chromosphere and, if it were small, would permit the Balmer and Paschen edges to appear in the spectrum (though diluted). The logic behind this theory rests upon steady-state one-dimensional atmospheric modeling, so that if spatial structure on the scale of the chromosphere/photosphere height difference exists, spatial structure will appear in the backwarmed photosphere; similarly, time variations would introduce discrepancies between the chromospheric UV source and the photospheric response.

In this paper, we address the essential property of optical depth directly, by the analysis of *SOHO*/MDI[3] images of the well-observed flare of 2002 July 15. The essence of the technique is simply to correlate the known intensity structure of the photosphere at the location of the flare brightening with the brightening itself and to interpret this in terms of a simple slab model for the radiative transfer (e.g., Boyer et al. 1985). To our knowledge, no analysis of this kind has been carried out before.

2. THE X3 FLARE OF 2002 JULY 15

This flare (GOES class X3) famously showed a multi-turn helical structure formed in its plasma ejection, as observed in *Transition Region and Coronal Explorer* (*TRACE*) UV images thought to represent mainly C IV emission (Liu et al. 2003). The chromospheric and photospheric properties of the event were recorded with Mees Observatory imaging spectroscopy in Hα and with white-light imagery from the Imaging Vector Magnetograph at Mees (Li et al. 2005). Unfortunately, *RHESSI* was at orbit night during the impulsive phase, so there are no hard X-ray images available, but Owens Valley microwave data were available. Figure 1 arrays the flare white light, soft X-ray, and OVSA 1–18 GHz microwave emissions as time series for reference; Li et al. have estimated energy fluxes for this comparison. To define the impulsive phase, Figure 1 also shows the GOES time derivative, since *RHESSI* hard X-ray data were not available.

The data we utilize in this study are the MDI "pseudo-continuum" intensity data, actually narrow-band samples of the continuum near the magnetically sensitive photospheric absorption line of Ni I at 6768 Å (Ding et al. 2003). The basic data are 1024 × 1024 time-averaged images at 1 minute cadence in a 10.′5 square field of view at disk center (pixel size 0.″615; diffraction limit $1.22\lambda/D = 1.''36$). The telescope has excellent pointing stability, and the noise in a given pixel is predominantly solar in origin—broad-band variations from convective motions, plus the *p*-modes. Figure 2 shows the images.

Our analysis focuses initially on the crescent-shaped flare region visible clearly in the 20:30 UT image (frame 2 of Figure 2). We then extend the technique to a generalized case. This part of the July 15 flare is particularly easy to analyze as it has the advantage of passing over regions with a wide range of

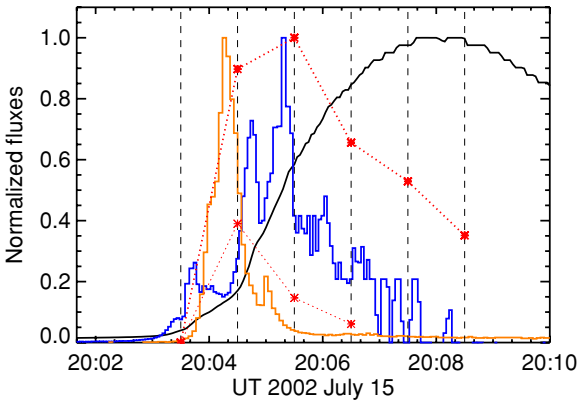

Figure 1. Time histories for the flare of 2002 July 15, normalized to the individual maxima. The thin black line is GOES 1–8 Å, and the blue line is its time derivative. The red points are white-light fluxes, total (upper) and the ribbon-like feature only (lower), both scaled to the peak of the total; the vertical dashed lines show the times of the white-light integrations. The orange line is the OVSA 18 GHz flux density.

(A color version of this figure is available in the online journal.)

photospheric intensities, and it proves simple to construct a low-noise photospheric background for it. The continuum emission has an elongated structure which might be misinterpreted as a loop in projection, but which the multiwavelength observations of Li et al. (2005) show clearly to be the eastern ribbon of the flare (see their Figure 7, in particular the frames showing the Hα blue wing at 20:03:32 and 20:04:01 UT for reference). Distributions of the intensity along an arc defining the midpoint of this ribbon source and along the same path on the preflare image (1 minute prior) are shown in Figure 5; these will be used together with a simple model to argue that the flare optical depth is small. However, a first indication that this is the case is simply that the photospheric structure is clearly superposed on the flare image.

3. SIMPLE MODEL

Our simple model of the radiative transfer in the white-light flare, shown in Figure 3, consists of an emission region (optical thickness τ and source function S_1) located above an optically thick photosphere at temperature T_0. This analysis follows that of Boyer et al. (1985). In the model, all intensities are dimensionless and scaled by dividing by the mean photospheric intensity. We assume that the photosphere (in a given pixel) has intensity $I_0 = S_0$ before the flare, where S_0 is the source function (the Planck function if in local thermodynamic equilibrium (LTE)). Here we explicitly ignore backwarming (see Section 1), assuming that the photosphere does not change significantly during the flare. As will be seen, this does not contradict the data we discuss for this flare. The observed intensity of a given pixel during the flare is I_F, which in this model consists of a combination of (attenuated) photospheric emission and direct flare emission. The observed brightness during the flare is generally given by

$$I_F = I_0 e^{-\tau} + S_1(1 - e^{-\tau}), \quad (1)$$

where S_1 is the source function for the flaring emission layer.

Is it possible to infer the optical depth τ of the flare from observations of the intensity of the flare emission? To illustrate this, consider the effect of changing the optical depth of a simple simulated flare, shown in Figure 4, overlaid onto a model photosphere that is constant in time. The model photosphere

[3] The Michelson–Doppler Imager (Scherrer et al. 1995) on board the *Solar and Heliospheric Observatory* (*SOHO*).

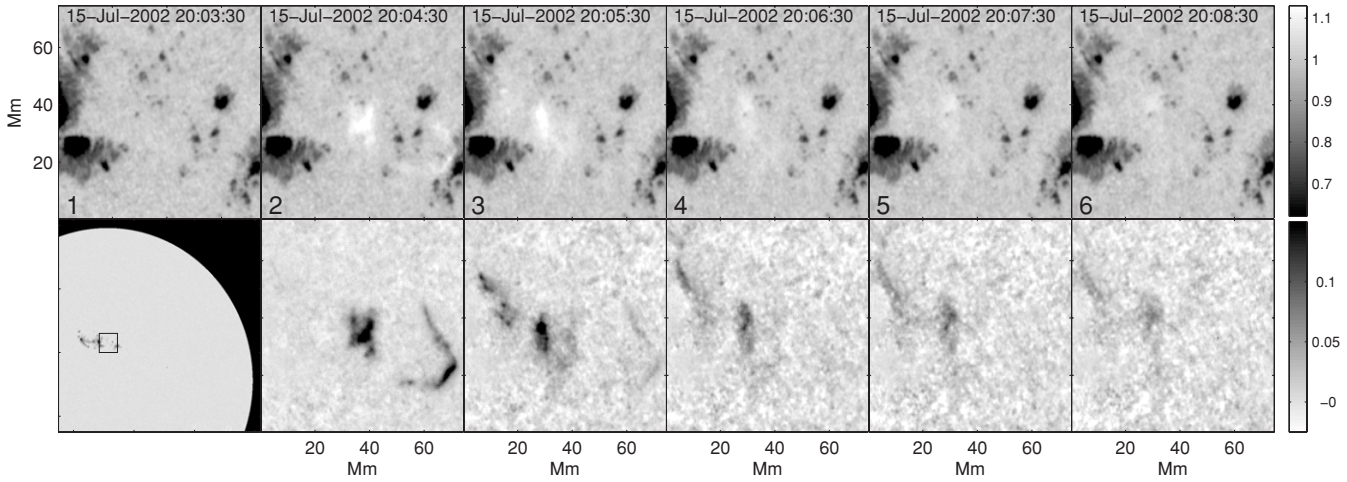

Figure 2. Time evolution of the flare at 1 minute cadence. The upper images show the flat-field-corrected MDI continuum images, and the lower images show the difference between these and a background photospheric image reconstructed by interpolation, color table reversed for clarity.

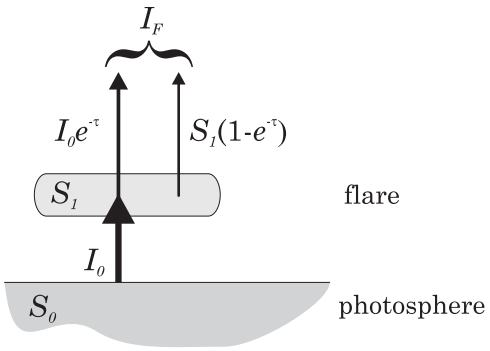

Figure 3. Cartoon representation of the flare geometry; a slab with limited horizontal scale overlying an unperturbed photosphere. The total emission from the flare I_F is the sum of the optically thick photospheric emission, attenuated by the optical depth of the flare region, and the emission from the flare region itself with source function S_1 and optical depth τ.

contains weak modulations patterned after granules and a dark "pore" region. In each case, the spatial variation of the flare emission $S_1(1-e^{-\tau})$ has the same Gaussian cross section, but the amplitude of the emission is chosen to give a peak brightening of the photosphere of 1.2 times the preflare intensity.

The lower graphs show the observed total emission I_F before (blue) and during (green) the flare, and the upper graphs (red) show the increase in intensity caused by the flare. In the case with large optical depth ($\tau = 1$), the photospheric emission is significantly attenuated when observed through the flare and so appears with a lower amplitude superimposed on the flare emission. If the photospheric emission is subtracted from the total flare emission, then the result is a combination of the flare emission with an inverted image of the photosphere, having a negative correlation with the original photosphere, which can be clearly seen in the upper left graph. The right-hand column shows the case where the flare has very small optical depth ($\tau = 0.01$). In this case, the total emission during the flare is approximately the sum of the unattenuated photospheric emission and the flare emission. When the photospheric background is subtracted from the flare, the result is almost exactly the true flare intensity profile, with no inverted component from the photosphere. It can be seen from this that if it is possible to know the intensity of the photosphere underlying the flare then the optical depth of the flare can be determined directly from the degree of spatial correlation between the flare brightening and the background image.

The analysis aims at determining the two unknown quantities τ and S_1 at each pixel of the continuum brightening. As we cannot assume LTE (see, e.g., Mihalas 1978), there is no simple relation between the emission, temperature, and opacity. We deal with this here by using the heuristic approximation described in the following section.

4. ANALYSIS

4.1. Heuristic Opacity Model

In the case that τ is small, we can simplify Equation (1) by taking a linear expansion of the exponential function $e^{-\tau} \approx 1 - \tau$:

$$I_F \approx I_0(1 - \tau) + S_1\tau. \quad (2)$$

This approximation gives errors of less than 4% for $\tau < 0.25$ and less than 0.5% for $\tau < 0.1$.

That τ must be small in our case is indicated by the upper right panel of Figure 5, where the photospheric intensity is subtracted from the flare frame; this is also shown as an image in the lower left panel. If the flare were significantly optically thick then the variations on the attenuated photosphere viewed through the flare would be smaller than those viewed directly, and therefore this difference image would contain an inverted representation of the photosphere, as can be seen in the left and middle columns of Figure 4. The absence of this tells us that the optical depth τ must be small, and furthermore that the background photosphere has not varied drastically during this minute.

As both τ and S_1 are unknown, Equation (2) cannot be solved from just the knowledge of I_F and I_0. We therefore need to postulate a heuristic relationship between τ and S_1, which is related to the physics of the emission and absorption in the slab region to make the problem tractable. If the physical situation in the source region (the slab) is characterized by overionization (Hudson 1972) and heating, we would expect τ and S_1 to correlate with each other, although the overionization would tend to increase the departure coefficient for the continuum and hold the temperature T_1 to a lower level. The simplest relationship would be τ = const., but this is clearly too restrictive; it would require that faint flares perfectly match the photosphere.

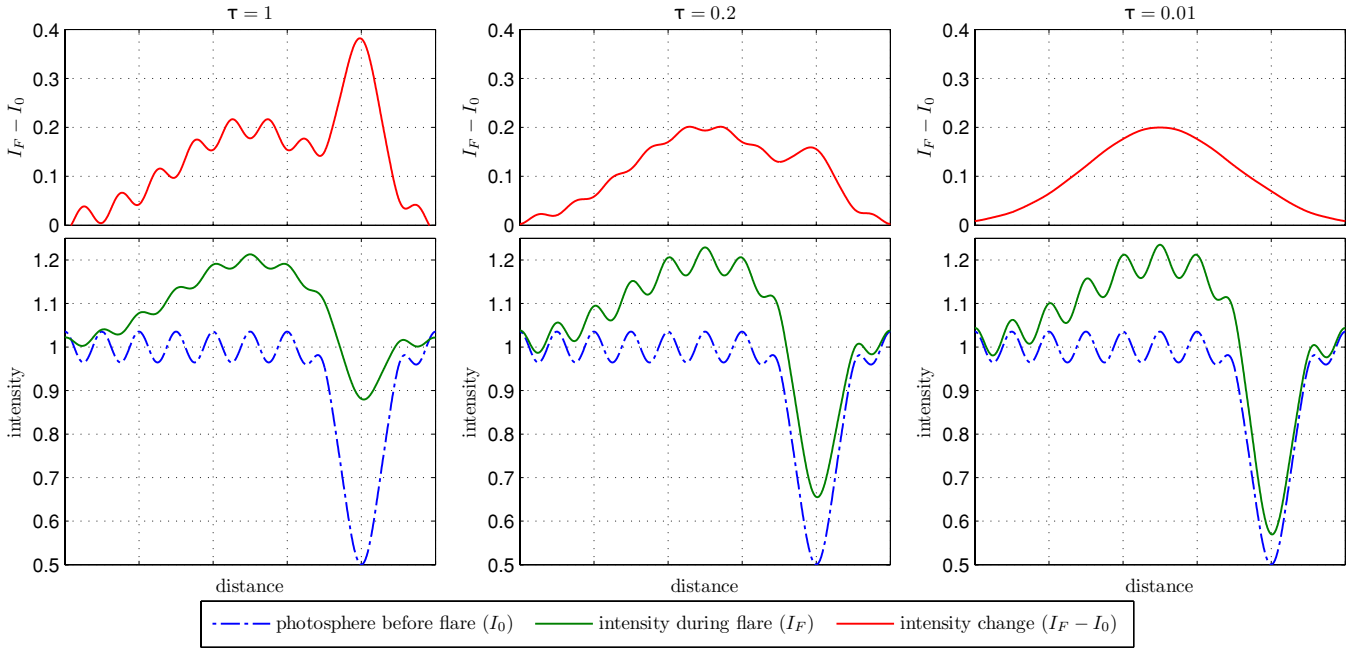

Figure 4. Simulated white-light flare emission profiles compared to the underlying photospheric emission for different values of the optical depth τ (from left to right, $\tau = 1, 0.2, 0.01$). The variations on the photosphere represent granules and a small sunspot, and all intensities are normalized to the mean photospheric intensity.
(A color version of this figure is available in the online journal.)

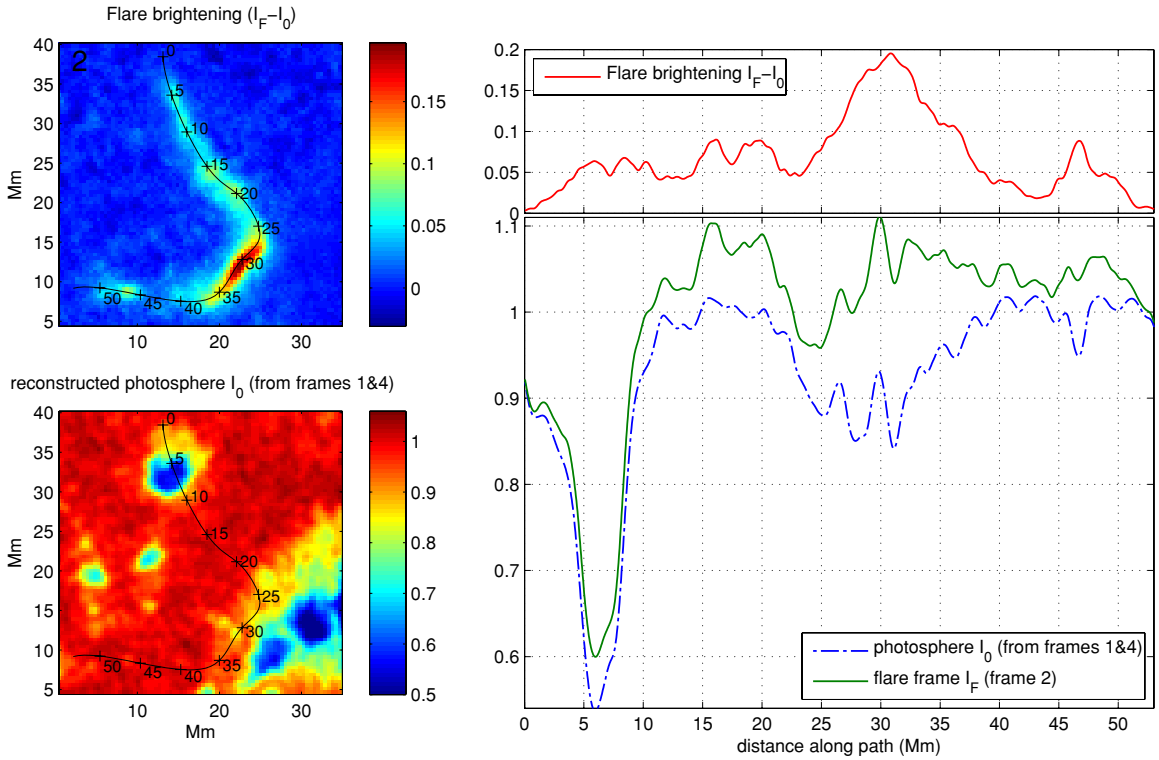

Figure 5. Intensity profile along the selected part of the flare, based on image frame 2 (20:04:30 UT). Left upper: the flare brightening excess; left lower: the photospheric structure underlying the emission; right: traces along the structure. Here, green shows the flare brightening, blue the reconstructed photosphere, and red the flare excess as in the simulations shown in Figure 4.
(A color version of this figure is available in the online journal.)

We have therefore adopted the relationship $\tau = \alpha(S_1 - I_0)$, where α is an unknown constant across all pixels as the simplest dependence of opacity on the physical conditions in the source. This relationship assumes that the optical depth of the flare region is proportional to the difference between the source function of the flare layer and the photosphere. In the absence of additional flare heating, the layer just above the photosphere will have a temperature closely related to the photospheric temperature. Particle heating of the layer would generally be expected to increase both the temperature (hence

source function) and the ionization fraction (hence optical depth), leading to strong continuum radiation, e.g., in the Balmer free-bound continuum. The relation above makes the simplest assumption that these two effects are of equal magnitude.

With this heuristic relationship, we find a quadratic equation for S_1 and solve it as

$$S_1 = I_0 + \sqrt{\frac{I_F - I_0}{\alpha}}. \quad (3)$$

The value of the constant α, which sets the optical depth, is unknown, but we can determine it by considering the spatial distribution of the flare emission. Note that α is not the optical depth itself, but a parameter describing its physics. Recall our assertion that the flare intensity is not correlated with the underlying photospheric intensity before the flare. The flare source function S_1 can be calculated using Equation (1) for a range of values of α and hence τ. If the variation of this derived flare source function is compared to the intensity of the underlying photosphere interpolated between preceding and following image frames, the two should be uncorrelated (except for random coincidence) when the correct optical depth is used in the calculation.

4.2. Estimation of the Parameter α

The key to the method described above is to observe the attenuation of the photospheric variation when viewed through the flare. In order to do this, we need to identify regions where the following are true.

1. We must be able to determine the underlying photospheric emission at the time of the flare. This requires reconstructing the photosphere by interpolating between non-flare image frames. The error of this interpolation can be estimated by comparing the reconstruction to the observed photosphere in regions outside the flare.
2. There must be significant spatial variation in the photospheric intensity over the flare region, which is much larger than the error on our photospheric reconstruction.
3. There must be significant flare brightening, again, much larger than the noise on the photospheric reconstruction.
4. The variation of the photospheric intensity needs to be as large as possible in comparison to the cospatial intensity variation of the flare at the scales considered. This is necessary to reduce the effects of chance correlations.

The flare cross section shown in Figure 5 is a particularly good example that meets these criteria. In this case, the reconstructed photospheric background was particularly accurate as it could be generated by a linear interpolation between image frames 3 and 6 (see Figure 2) due to the rapid evolution of the flare brightening. The error on this reconstruction was ∼0.5% of the mean photospheric intensity, estimated from the difference between the reconstructed photosphere and the observed photosphere in regions away from the flare.

The profiles of the observed emission before (I_0) and during (I_F) the flare and the brightness increase ($I_F - I_0$) are shown in the right-hand panel of Figure 5. The variation of the flare source function S_1 was then calculated using the reconstructed photospheric intensity I_0 and Equation (3) for a range of different values of the opacity parameter α, and the correlation between this and the photospheric background was calculated. Recall that the aim of calculating the correlation is to determine exactly the amplitude of the photospheric variations when viewed through the flare. In order to maximize the statistical validity of this correlation calculation, we need as many independent data points as possible. Unfortunately, due to the large-scale features present in both the photosphere and the flare brightening, clearly visible in Figure 5, points taken along this profile are far from independent and a simple correlation would tend to reflect the chance alignment of these large-scale features.

Table 1
Summary of the Results from Different Image Frames

Frame	α	Mean (τ)	rms error (%)	$\Delta S/S$[a]
2	0.0037	0.015	0.78	8.5
3	0.0131	0.033	1.17	11.5
4	0.0309	0.042	1.28	7.2
5	0.0119	0.024	1.31	5.9
6	0.0233	0.032	1.35	5.2
7	0.0066	0.016	1.32	4.7
All		0.028		

Note. [a] $\Delta S/S$ is the percentage flare excess brightness, from the selected regions, normalized to the non-flaring photosphere.

This problem can be ameliorated by applying a high-pass spatial filter to both the reconstructed photosphere and the modeled flare emission before calculating the correlation between them. This filter should be chosen to preserve as much photospheric variation as possible while removing the large-scale autocorrelation from the data, thus creating the maximum number of independent measurements. In the data used here, much of the photospheric variation is close to the resolution limit of MDI (1.″36, ≈1 Mm), so a fairly tight high-pass filter with 3.5 Mm FWHM could be used, and regions where the photospheric variation on the filtered data was large were chosen manually. These are shown by the bold portions of the filtered cross section shown in Figure 6.

Figure 6 gives the results, with reconstructions for $\alpha = 0.01$ and $\alpha = 0.004$ shown in the left panels, and the variation of the correlation with α shown on the right-hand panel. It can be seen that for the $\alpha = 0.25$ case, the generated flare profile shows a significant positive correlation with the underlying photosphere, which completely disappears when α is small. According to the arguments in Section 3, this implies small optical depths. In this case, the correlation goes to zero when $\alpha = 0.0036$. From our assumption that $\tau = \alpha(S_1 - I_0)$, this gives an average optical depth for the flare of $\tau = 0.028$, with the variation of τ along the path shown in the lower panel.

The above example indicates very small optical depth, but since the method assumes no correlation between the detailed photospheric intensity and the flare brightening, random correlations could also give that result. To test this, we need to look at a larger data set. To automate this, algorithms were constructed that isolated the regions where the four criteria listed above were true. An example of this from frame 2 is shown in Figure 7. This process was carried out for all image frames and the results are summarized in Table 1. As can be seen, the mean optical depth of the flares in each frame is small, with a maximum of 0.042. Notice that the value of τ is not related to the average flare brightening and is lowest for the frame which has the lowest photospheric error (image frame 2).

4.3. Error Analysis

The major error source in the above procedure is the error in the estimate of the photospheric brightness in regions under flare regions. Although the average of this error will be zero

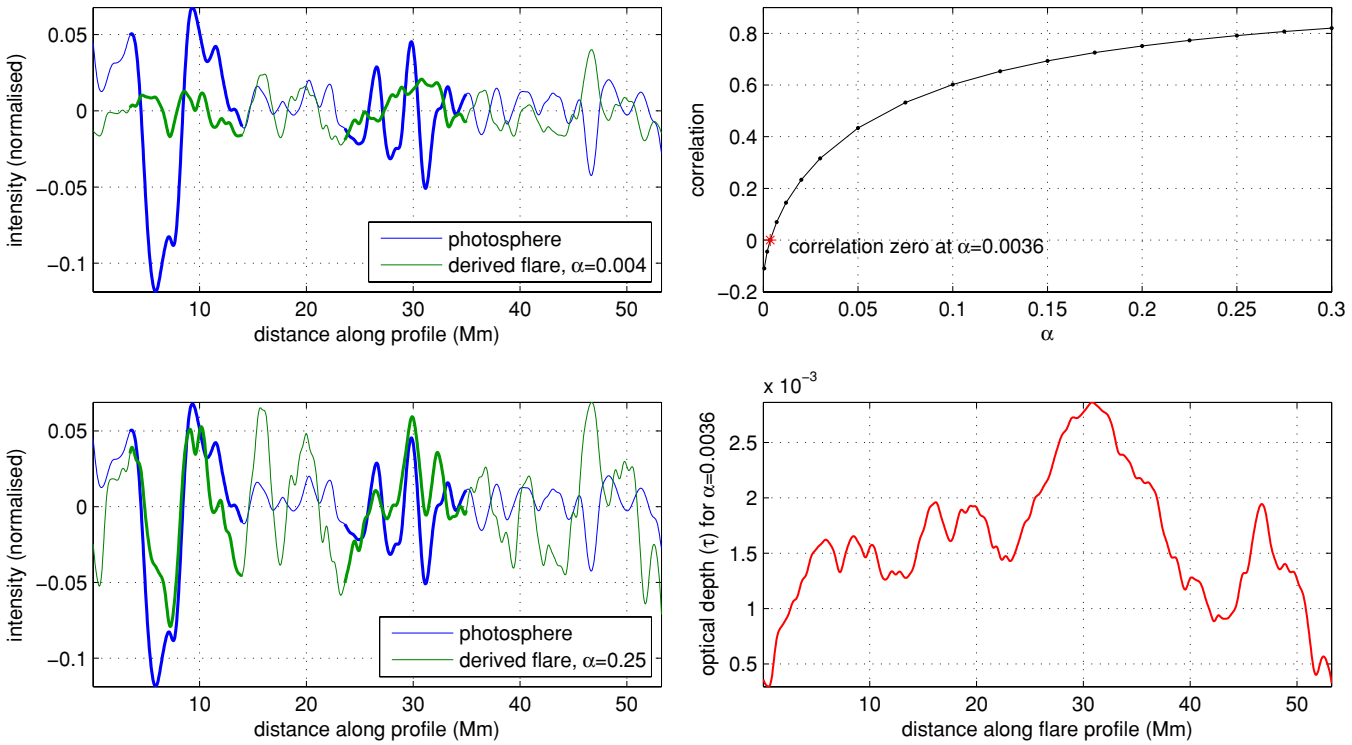

Figure 6. Left: calculated flare intensities for $\alpha = 0.004$ and $\alpha = 0.25$ for the path shown in Figure 5, after passing through a high-pass filter with cutoff of 3.5 Mm FWHM. The bold line sections are the regions selected for the correlation calculations where significant flare brightening is combined with large photospheric variation. Notice the significant correlation between the derived flare intensity and the photosphere intensity for the $\alpha = 0.25$ case. Right: correlation of the derived flare intensity with the underlying photospheric emission as a function of the opacity parameter α. The correlation is zero for $\alpha = 0.0038$, and the lower panel shows the optical depth of the derived flare for this value of α.

(A color version of this figure is available in the online journal.)

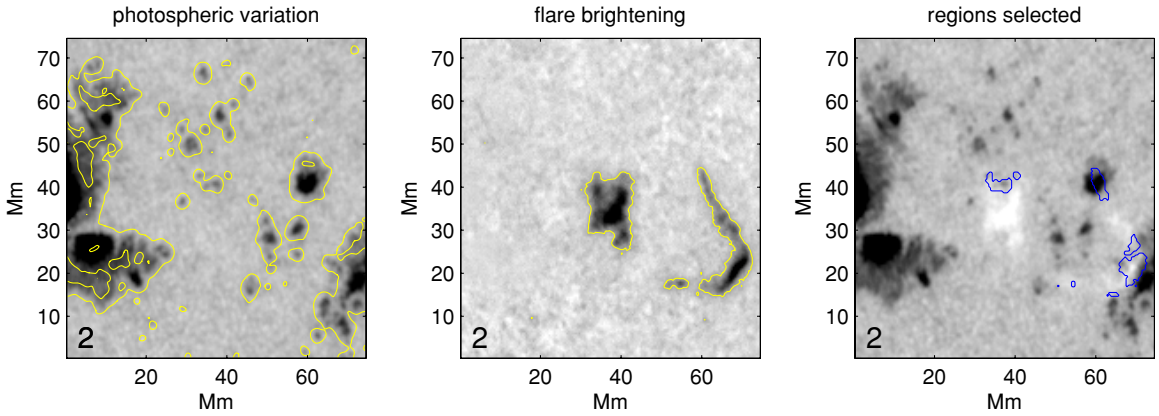

Figure 7. Selection of regions for analysis. Left: map of the photospheric rms variability; middle: difference image showing the flare brightening, with contours showing the selected regions; right: the intersection of these selections for analysis.

(A color version of this figure is available in the online journal.)

by assumption, the spurious structure it introduces to the photospheric reconstruction gives a systematic error to the derived value of α, and hence to the derived optical depth, always tending to increase the derived value. To see why this should be true, consider the effect of adding a pattern of random noise to the reconstruction of the photosphere underlying the flare. The observed intensity of the solar surface with the flare present will not contain this error term, so it will appear that the flare is masking it, suggesting that it is more optically thick than is really the case.

In order to evaluate the significance of the photospheric noise, we add noise of various (known) amplitude levels to the reconstructed photosphere. First, the rms error on the photospheric reconstructions was measured for each image frame by comparing the reconstructed photospheric image in a region away from the flare emission to the observed photosphere; results are shown in Table 1. Normally distributed noise with a range of known standard deviations was then added to the reconstructed photosphere and the calculation of α repeated. This was done multiple times with different random noise for each frame and each value of the noise amplitude, in order to avoid random correlations between added noise and the photosphere. The variation in the derived value of α versus the total photospheric error for each frame is shown in Figure 8. It

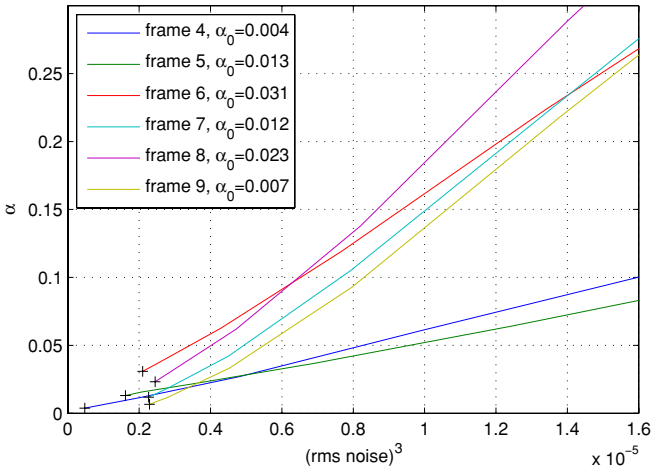

Figure 8. Effect of noise in the photospheric reconstruction on the derived value for α. Extrapolating this graph back to the y-axis allows the zero noise case to be estimated.

(A color version of this figure is available in the online journal.)

can be seen that as the error in the photospheric noise increases, the derived value of α also tends to increase as expected. Note that the values of α determined in image frames where the flare brightness is larger (see Table 1) are much less sensitive to the effect of the noise.

Using this graph, it is possible to extrapolate back to a "zero error" value for α. If this is done for each frame using a simple polynomial extrapolation, we get an average value for all the data of $\alpha = -0.0001 \pm 0.01$, so to within the accuracy of these measurements the optical depth is effectively zero.

4.4. Discussion

Our direct analysis of the flare emission from seven image frames, comprising a total of 1200 pixels where the flare emission significantly enhanced the surface brightness, has given us the result that the optical depth is 0.028 ± 0.01. This value however should be regarded as an upper limit on the opacity of the flaring regions; when the effect of photospheric noise is considered, the optical depth becomes too small to measure and certainly less than 0.01.

As a result of this, the assumption of our heuristic opacity model that τ depends on the flare source function becomes unimportant, as the optical depth is so close to zero that a more appropriate model for the emission becomes

$$I_F = I_0 + I_1, \quad (4)$$

where I_1 is the flare emission. It simply adds to the photospheric emission.

We note that an idealized backwarming model for the flare brightening would also match this observation, but we can rule this out because of the fine structure present in the flare image. Isobe et al. (2007) discuss this aspect of white-light flare geometry in detail. In our model, the height of the slab is comparable to the width of the ribbon-like flare emission, which varies substantially along its length and is unresolved in its narrowest parts. Furthermore, the flare region we discuss has a lifetime less than 60 s, whereas the cooling time in the VAL_C model (Vernazza et al. 1981) is about 80 s at the photosphere; we calculate the timescale as $\varepsilon \mathrm{H}/\mathcal{L}_\odot$, where ε, H, and $\mathcal{L}_\odot$ are the thermal energy density, scale height of the photosphere, and photospheric luminosity, respectively. This is not a decisive argument because of the low time resolution of our observations.

5. CONCLUSIONS

If we assume that the origin of the flare emission is predominantly from an excited region above the photosphere, rather than enhanced photospheric emission from backwarming, then we have shown that the emission from this overlying region is optically thin. This can be seen from the fact that the amplitude of photospheric variations that can be seen through the flare is unchanged in comparison to the photosphere before and after the flare. That backwarming is not significant as indicated by (1) the observations of Isobe et al., which show bright structures down to *Hinode* angular scales of 0.″2–0.″3; (2) the fact that we see unresolved structures down to ∼1 Mm; and (3) the remark that it is unlikely that the backwarming physics would be the same over a pore and over the quiet photosphere, due to the different optical depths, temperatures, and transport properties of the photosphere. Any difference in the backwarming which is a function in the photospheric structure would appear in this analysis as an increased (or negative) optical depth. As the optical depth comes out to be almost exactly zero, this does not seem likely.

The optical depth of the white-light flare regions we have studied is very small, indistinguishable from zero in this study, and in any case less than ∼0.01. We infer from this that the flare must be of low density and hot, almost certainly far from LTE. The temperature cannot be determined from this but is generally constrained by the new flare bolometric observations (Woods et al. 2004; Kretzschmar et al. 2010; Quesnel et al. 2010); many authors suggest a value near 10^4 K (e.g., Hudson et al. 2010). These results definitely tend to reduce the importance of photospheric backwarming in our understanding of white-light flare emission.

Because the MDI data represent averages over 1 minute intervals and because they represent only a narrow slice of the true continuum, this result should be considered as a preliminary one. Newer data with better image cadence and spatial resolution (*Hinode* or *SDO* in space, or a variety of ground-based instruments leading up to ATST) should be applied to this interesting problem. If confirmed, this result suggests that the generally accepted picture of flare energy storage in the corona, with flare effects in the lower atmosphere derived from this energy reservoir, must be correct. Note that this is the usual assumption, but it has not been easy to establish observationally.

This work is supported by the EU SOLAIRE Research and Training Network at the University of Glasgow (MTRN-CT-2006-035484) and by Rolling Grant ST/F002637/1 from the UK Science and Technology Facilities Council and the Leverhulme Trust, Research Grant number F/00 179/AY. H.H. also thanks NASA for support under contract NAS 5-98033 for *RHESSI*.

REFERENCES

Aboudarham, J., & Henoux, J. C. 1986, A&A, 156, 73
Boyer, R., Sotirovsky, P., Machado, M. E., & Rust, D. M. 1985, Sol. Phys., 98, 255
Brown, J. C., Turkmani, R., Kontar, E. P., MacKinnon, A. L., & Vlahos, L. 2009, A&A, 508, 993
Ding, M. D., Liu, Y., Yeh, C.-T., & Li, J. P. 2003, A&A, 403, 1151

Fletcher, L., Hannah, I. G., Hudson, H. S., & Metcalf, T. R. 2007, ApJ, 656, 1187
Fletcher, L., & Hudson, H. S. 2008, ApJ, 675, 1645
Hudson, H. S. 1972, Sol. Phys., 24, 414
Hudson, H. S., Acton, L. W., Hirayama, T., & Uchida, Y. 1992, PASJ, 44, L77
Hudson, H., Fletcher, L., & Krucker, S. 2010, arXiv:1001.1005
Isobe, H., et al. 2007, PASJ, 59, 807
Kretzschmar, M., de Wit, T. D., Schmutz, W., Mekaoui, S., Hochedez, J. F., & Dewitte, S. 2010, Nat. Phys., 6, 690
Li, J., Mickey, D. L., & LaBonte, B. J. 2005, ApJ, 620, 1092
Liu, Y., Jiang, Y., Ji, H., Zhang, H., & Wang, H. 2003, ApJ, 593, L137
Machado, M. E., Emslie, A. G., & Avrett, E. H. 1989, Sol. Phys., 124, 303
Machado, M. E., Emslie, A. G., & Mauas, P. J. 1986, A&A, 159, 33
Metcalf, T. R., Alexander, D., Hudson, H. S., & Longcope, D. W. 2003, ApJ, 595, 483
Mihalas, D. 1978, Stellar Atmospheres (2nd ed.; San Francisco, CA: Freeman)
Najita, K., & Orrall, F. Q. 1970, Sol. Phys., 15, 176
Neidig, D. F. 1989, Sol. Phys., 121, 261
Neidig, D. F., & Kane, S. R. 1993, Sol. Phys., 143, 201
Neidig, D. F., & Wiborg, P. H., Jr. 1984, Sol. Phys., 92, 217
Quesnel, A., Dennis, B. R., Fleck, B., Froelich, C., & Hudson, H. S. 2010, arXiv:1003.4194
Rust, D. M., & Hegwer, F. 1975, Sol. Phys., 40, 141
Scherrer, P. H., et al. 1995, Sol. Phys., 162, 129
Švestka, Z. 1970, Sol. Phys., 13, 471
Unsöld, A. 1968, QJRAS, 9, 294
Vernazza, J. E., Avrett, E. H., & Loeser, R. 1981, ApJS, 45, 635
Woods, T. N., et al. 2004, Geophys. Res. Lett., 31, 10802
Xu, Y., Cao, W., Liu, C., Yang, G., Jing, J., Denker, C., Emslie, A. G., & Wang, H. 2006, ApJ, 641, 1210
Xu, Y., Cao, W., Liu, C., Yang, G., Qiu, J., Jing, J., Denker, C., & Wang, H. 2004, ApJ, 607, L131